Perovskite Defects

International Edition: DOI: 10.1002/anie.201507729
German Edition: DOI: 10.1002/ange.201507729

Trapping of Oxygen Vacancies at Crystallographic Shear Planes in Acceptor-Doped Pb-Based Ferroelectrics

*Dmitry Batuk, Maria Batuk, Alexander A. Tsirlin, Joke Hadermann, and Artem M. Abakumov**

Abstract: *The defect chemistry of the ferroelectric material $PbTiO_3$ after doping with Fe^{III} acceptor ions is reported. Using advanced transmission electron microscopy and powder X-ray and neutron diffraction, we demonstrate that even at concentrations as low as circa 1.7% (material composition approximately $ABO_{2.95}$), the oxygen vacancies are trapped into extended planar defects, specifically crystallographic shear planes. We investigate the evolution of these defects upon doping and unravel their detailed atomic structure using the formalism of superspace crystallography, thus unveiling their role in nonstoichiometry in the Pb-based perovskites.*

Perovskite-based ferroelectrics are widely applied in modern technologies because their dielectric properties can be tuned by appropriate doping.[1] Doping of $Pb[Zr_xTi_{1-x}]O_3$ (ABO_3) with acceptor atoms (B cations with an oxidation state lower than +4) causes "hardening" of the material, making it suitable for producing actuators or resonators. Owing to the technological importance, the microscopic mechanism of doping has been actively studied both experimentally and theoretically. Replacement of Ti^{IV} or Zr^{IV} by an acceptor cation introduces oxygen vacancies which form a defect associate with an acceptor atom. When a few atom% of Fe^{III} ions are doped into the $PbTiO_3$ or $Pb[Zr_xTi_{1-x}]O_3$ ceramics, the defect associate can be expressed using the Kröger–Vink notations as $(Fe'_{Ti}-V_O^{\bullet\bullet})^{\bullet}$ (the prime and dot denote the charges of −1 and +1, respectively).[2–6] Since the overall charge of the defect associate is +1, negatively charged lead vacancies V''_{Pb} are required for charge compensation, and therefore lead deficiency is assumed.[4] The segregation of oxygen vacancies becomes particularly important in the context of Scott and Dawber's conjecture on the oxygen-vacancy ordering as a polarization fatigue mechanism in perovskite ferroelectrics.[7] Polarization fatigue, the degradation of remnant polarization upon repetitive switching, is related in this model to electromigration of randomly distributed oxygen vacancies and their ordering into planar arrays pinning ferroelectric domain wall motion.[8] The behavior of diluted oxygen vacancies is usually weakly correlated, and the oxygen-vacancy-based fatigue mechanism assumes that they interact only above a certain concentration limit, which is estimated to be approximately 7% ($ABO_{2.80}$). The exact ordering pattern of point oxygen vacancies is not yet clear and their role in the polarization fatigue is still under debate.[9–11] In this Communication, we report on the peculiarities of the defect chemistry when Fe^{III} acceptor ions are doped into ferroelectric $PbTiO_3$. We demonstrate that even at a vacancy concentration as low as circa 1.7% (composition ≈ $ABO_{2.95}$) the oxygen vacancies are trapped into extended planar defects, namely crystallographic shear (CS) planes. Although the formation of CS planes in ferroelectric perovskites was put forward 40 years ago, neither their direct experimental observation nor their structure have been reported.[12] Herein, we investigate the evolution of these planar defects upon doping, unravel their atomic structure, and explain their possible role in the Pb and O deficiency in acceptor-doped Pb-based ferroelectrics.

The $Pb_{1-x}(Ti_{1-z}Fe_z)_{1+x}O_{3-y}$ ($0 \le z \le 1$) materials were prepared by a solid-state reaction at 860–1100 °C, with the annealing temperature rising concomitantly with the Ti content (see the Experimental Section and Tables S1, S2 in the Supporting Information). X-ray powder diffraction (XPD) patterns of $Pb_{1-x}(Ti_{1-z}Fe_z)_{1+x}O_{3-y}$ demonstrate systematic changes with increasing Fe^{III} content: the tetragonal distortion of the perovskite unit cell diminishes and progressive anisotropic reflection broadening occurs for z values up to 0.15, followed by reflection splitting and the appearance of extra peaks above $z = 0.2$ (Figure S1–S3). This behavior is indicative of extended defects that form an ordered pattern at higher z values. In the high-angle annular dark-field scanning transmission electron microscopy (HAADF-STEM) images of the prepared compounds (Figure 1), the most eye-catching feature is the arrangement of the bright dots corresponding to the Pb atomic columns: they form a perovskite square pattern separated into domains by the planar defects. The dots corresponding to the Ti/Fe-O columns are weaker. At low Fe^{III} concentration ($z = 0.1$), the defects occur randomly in the perovskite matrix, but are confined to the $(101)_p$ or $(10\bar{1})_p$ perovskite planes. At $z = 0.2$, the defects demonstrate correlated behavior: they tend to align parallel to the $(101)_p$ plane equidistantly spaced by about 60 Å. Owing to weak interaction between defects, their orientation and interplanar spacing vary locally and result in a wavy appearance. With a further increase of the Fe^{III} content up to $z \approx 0.975$, a regular

[*] Dr. D. Batuk, Dr. M. Batuk, Prof. Dr. J. Hadermann, Dr. A. M. Abakumov
EMAT, University of Antwerp
Groenenborgerlaan 171, 2020, Antwerp (Belgium)
E-mail: artem.abakumov@uantwerpen.be
Dr. A. M. Abakumov
Chemistry Department, Moscow State University
119991, Moscow (Russia)
Dr. A. A. Tsirlin
National Institute of Chemical Physics and Biophysics
12618, Tallinn (Estonia)
and
Experimental Physics VI, EKM, University of Augsburg
86159 Augsburg (Germany)

Supporting information for this article is available on the WWW under http://dx.doi.org/10.1002/anie.201507729.

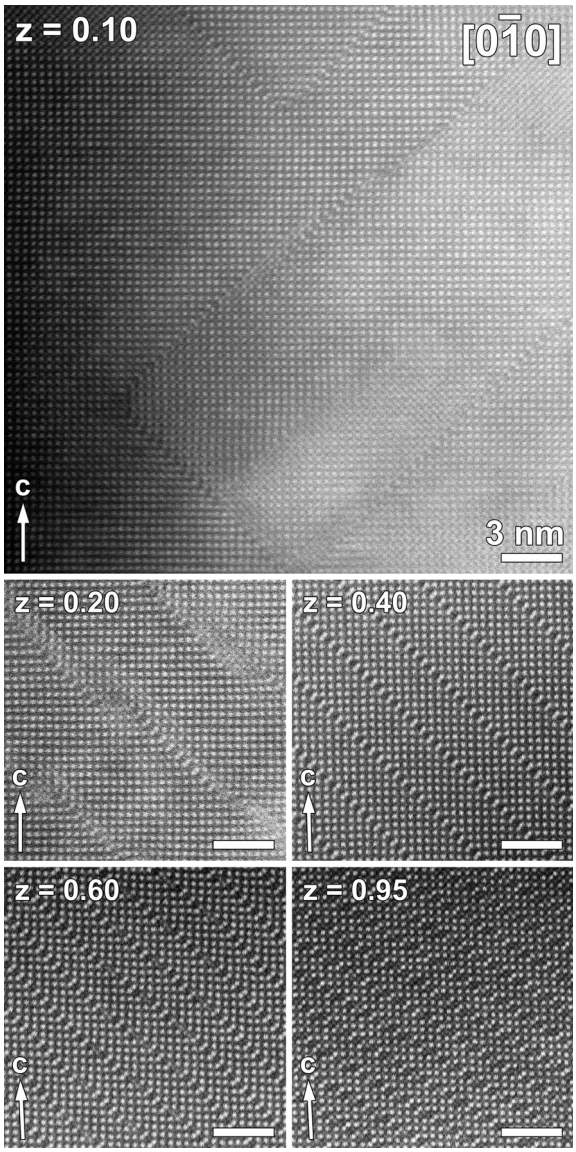

Figure 1. HAADF-STEM images of selected $Pb_{1-x}(Ti_{1-z}Fe_z)_{1+x}O_{3-y}$ materials. The orientations of the defect planes are approximately $(101)_p$ and $(10\bar{1})_p$ for $z=0.10$; $(101)_p$ for $z=0.20$, 0.40; $(\underline{1}0\underline{1}1)$ for $z=0.60$; $(70\underline{1}1)_p$ for $z=0.95$.

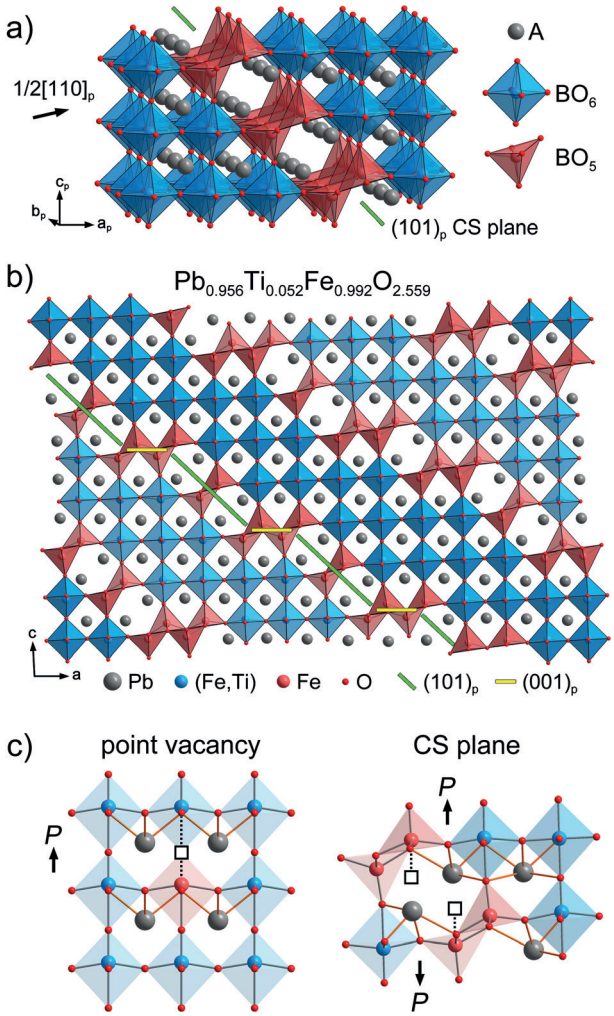

Figure 2. a) Schematic drawing of the $(101)_p$ CS plane in an ABO_3 perovskite structure. b) A representative $13a\times1b\times8c$ fragment of the $z=0.95$ refined structure. c) Comparison between two models for the Fe^{III} doping in $PbTiO_3$: defect associate $(Fe'_{Ti}-V_O^{\bullet\bullet})^{\bullet}$ formed by an oxygen vacancy (square) and the Fe^{III} ion in an incomplete FeO_5 polyhedron (red), in accordance with Refs. [6] and [19] and Fe^{III} segregation at the CS plane.

long-range order of the planar defects sets in. The thickness of the perovskite blocks between the defect planes decreases with increasing values of z and the orientation of the planes changes gradually from $(101)_p$ towards $(508)_p$. Finally, at high Fe^{III} content $(0.975<z\leq1)$ the materials form "$Pb_2Fe_2O_5$"-type highly defective structures.[13–15]

These planar defects can be identified as CS planes (by comparing the images in Figure 1 to those of perovskite CS structures in Refs.[16,17,18]). An $(h0l)_p$ CS plane is formed by displacement of one part of the ABO_3 perovskite structure with respect to another over a vector $^1/_2[110]_p$. The displacement transforms corner-sharing BO_6 octahedra along the plane into edge-sharing BO_5 tetragonal pyramids (Figure 2a). This reduces the oxygen content by trapping anion vacancies at the CS plane and changing the connectivity of the metal–oxygen polyhedra. The shear operation creates tunnels filled by double A cation columns.[13] These A positions with a highly asymmetric oxygen environment can only be occupied by stereochemically active lone-pair cations, such as Pb^{II} and Bi^{III}. For that reason, the CS mechanism cannot be envisaged in ferroelectrics like $BaTiO_3$.

The atomic structure of the defects is directly confirmed by the Rietveld refinement of the well-ordered $z=0.95$ crystal structure against neutron powder diffraction (NPD) data. As a result of the large relaxation at the CS planes, the structure is incommensurately modulated and we described it using a (3+1)D structural model developed for $(Pb,Bi)_{1-x}Fe_{1+x}O_{3-y}$.[16,18] The model also allows interpretation of the XPD data of other $Pb_{1-x}(Ti_{1-z}Fe_z)_{1+x}O_{3-y}$ members (see the crystallographic parameters in Table S3). The $z=0.95$ compound is antiferromagnetically ordered at room temperature. To avoid the magnetic contribution, the refinement was

performed using the NPD data at $T = 900$ K (Tables S4–S5; Figure S4-S5). A representative $13a \times 1b \times 8c$ fragment of the $z = 0.95$ structure is shown in Figure 2b. The CS planes in this material adopt an orientation close to $(70\underline{1}1)_p$. The $(h0l)_p$ CS plane can be considered as an ordered sequence of alternating $(001)_p$ and $(101)_p$ segments containing chains of distorted FeO_5 square pyramids sharing common basal edges. The $(101)_p$ and $(001)_p$ segments are based on double and quadruple pyramidal chains, respectively. The $(101)_p$ segments reduce the oxygen content, while $(001)_p$ segments also reduce the Pb/(Fe, Ti) ratio leading to the Pb deficiency. The $(h0l)_p$ orientation of the planes is related to the components of the modulation vector as $h/l = \alpha/\gamma$. Based on the (3+1)D structural model, the chemical composition can be expressed as $Pb_{1+\alpha-\gamma}(Ti_{1-z}Fe_z)_{1-\alpha+\gamma}O_{3-\alpha-3\gamma}$, with $x = \gamma - \alpha$ and $y = 3\gamma + \alpha$ in $Pb_{1-x}(Ti_{1-z}Fe_z)_{1+x}O_{3-y}$. The z parameter, which is the main parameter that governs the structure, is not directly present in the model, but can be estimated using the electroneutrality condition as $z = 8\gamma/(1-\alpha+\gamma)$.

Spatially resolved electron energy loss spectroscopy (EELS) and energy dispersive X-ray spectroscopy (EDX) demonstrate that the tetragonal pyramids at the CS planes are exclusively occupied by the Fe^{III} ions (Figure 3; Figure S6)

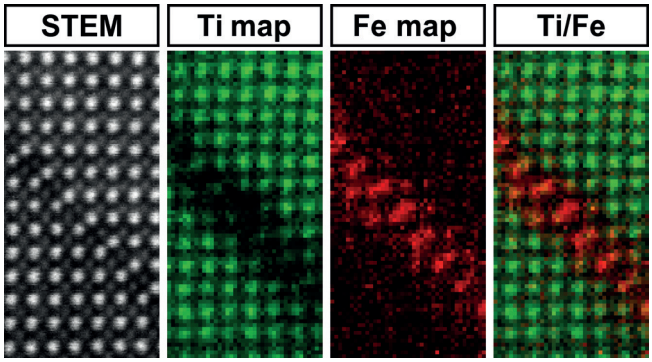

Figure 3. High-resolution STEM-EELS elemental maps of the $z = 0.2$ sample showing the Fe^{III} segregation at the CS plane.

segregating together with the oxygen vacancies, whereas the Ti^{IV} ions are located in the perovskite blocks. It could be argued that this segregation might originate from insufficient homogenization of the Fe^{III} dopant. To refute this argument, we prepared the $Pb_{1-x}(Ti_{1-z}Fe_z)_{1+x}O_{3-y}$ samples using chemical homogenization. The HAADF-STEM images of the $z = 0.05$ (1.7% of oxygen vacancies) and $z = 0.3$ samples (9.9% of oxygen vacancies; Figure S7, S8) clearly demonstrate the presence of the CS planes, showing that their formation is intrinsic to this system.

The local Fe–O atomic arrangement at the CS planes resembles the geometry of the $(Fe'_{Ti}-V_O^{\bullet\bullet})^{\bullet}$ polar defect associates (Figure 2c), whose dipoles are parallel to the bulk polarization.[20] Formation of the CS planes can be considered as tail-to-tail condensation of these defects, so that their dipoles become aligned antiparallel on either side of the CS plane. An ordered array of CS planes results in an "antipolar" structure, where the off-center cation displacements are largest at CS planes but oriented in the opposite directions and absent at the center of the perovskite blocks.[6,19] It is also noteworthy that the condensation of the defect associates might be sensitive to the synthetic method. The XPD patterns of the $PbTi_{1-z}Fe_zO_{3-\delta}$ solid solutions prepared using wet chemistry at 700 °C do not demonstrate the reflection splitting expected for the CS structure at least up to $z = 0.5$, but raising the annealing temperature to 850 °C and 1000 °C produces XPD patterns characteristic of CS planes.[21]

At high doping levels, Fe^{III}-doped $PbTiO_3$ develops antiferromagnetic order, which is seen in the room-temperature NPD pattern of the $z = 0.95$ sample (Figure S9). Temperature dependence of the magnetic susceptibility for the $z = 0.9$ sample indicates an antiferromagnetic transition with the Néel temperature of $T_N = 485$ K (Figure 4, bottom). In contrast, the $z = 0.3$ sample demonstrates an overall

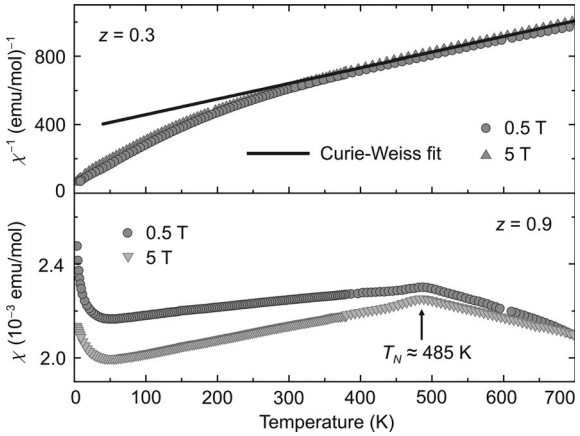

Figure 4. Top: Inverse magnetic susceptibility of the $z = 0.3$ sample and the Curie–Weiss fit above 400 K with the paramagnetic effective moment of 2.96 μ_B (26% of Fe^{III} ions) and an antiferromagnetic Curie–Weiss temperature $\theta = 400$ K. Bottom: Magnetic susceptibility of the $z = 0.9$ sample revealing an antiferromagnetic ordering transition at $T_N \approx 485$ K. The weak-field dependence may be due to trace amounts of a ferrimagnetic impurity, such as $PbFe_{12}O_{19}$ or Fe_2O_3.

paramagnetic behavior, but its inverse magnetic susceptibility follows the Curie–Weiss law above 400 K only, and the Curie–Weiss temperature θ is as high as 400 K (Figure 4, top). At $T < \theta$, exchange interactions between the Fe^{III} ions segregated at the CS planes may induce short-range magnetic order that results in deviations from the paramagnetic Curie–Weiss behavior. However, no long-range magnetic order is formed. No signatures of ferromagnetism have been observed for $z =$ 0.05, 0.1, 0.15, 0.2, and 0.3 samples (Figure S10, S11). On the other hand, antiferromagnetic interactions between the Fe^{III} ions affect the magnetic susceptibility at doping levels as low as 10%.

To summarize, the substitution of Ti^{IV} by Fe^{III} in $PbTiO_3$ leads to the condensation of the $(Fe'_{Ti}-V_O^{\bullet\bullet})^{\bullet}$ defect associates into CS planes at an oxygen vacancy concentration as low as about 1.7%. The CS planes occur as random defects at low Fe^{III} doping and demonstrate well-established long-range order at Fe^{III} concentrations above 20 atom%. The structure

of the CS planes reveals the microscopic mechanism behind the oxygen and lead deficiency in acceptor-doped Pb-based ferroelectrics. As a result of the tail-to-tail condensation of the $(Fe'_{Ti}-V_O^{\bullet\bullet})^{\bullet}$ defect associates, an ordered arrangement of the CS planes renders the structure antipolar. This direct information on the defect chemistry of perovskite ferroelectrics opens the door for further studies of extended defects and their influence on dielectric performance.

Experimental Section

Samples were prepared from PbO (Sigma–Aldrich, $\geq 99.9\,\%$), Fe_2O_3 (Sigma–Aldrich, $\geq 99.98\,\%$), and TiO_2 (Aldrich, $\geq 99.8\,\%$). The oxides were ground, pelletized, and annealed with intermediate regrindings under the conditions summarized in Table S1 in the Supporting Information. To compensate for the lead oxide volatility, 5 wt.% PbO was added on the second-last annealing. The soft-chemistry procedure was similar to that reported in Ref. [21], and the details are given in the Supporting Information.

The XPD patterns were acquired on a Huber G670 diffractometer ($Cu_{K\alpha 1}$ radiation). The NPD data were collected on the HRPT diffractometer at the Paul Scherrer Institute (LNS PSI, Villigen, Switzerland) at wavelength 1.8857 Å in the 2θ range 8–160° in a 8 mm vanadium container at 900 K. Crystal structure analysis was performed with JANA 2006.[22]

The TEM samples were prepared by crushing the powder in ethanol and depositing the suspension onto holey carbon TEM grids. HAADF-STEM images, STEM-EDX, and STEM-EELS maps were acquired on a FEI-Tecnai G2 microscope and an aberration-corrected FEI Titan^3 60–300 microscope equipped with a Super-X detector and a Gatan Enfinium ER spectrometer. The STEM-EDX and STEM-EELS data were recorded at 200 kV and 120 kV.

Magnetic susceptibility was measured using the vibrating sample magnetometer (VSM) insert of Quantum Design PPMS and the VSM SQUID MPMS 3 system. Measurements above 400 K were performed using the oven setup under high vacuum (10^{-5} torr).

Acknowledgements

A.M.A. is grateful to the Russian Science Foundation (grant 14-13-00680). A.A.T. acknowledges experimental support from Dr. Anton Jesche and funding by the Federal Ministry for Education and Research through the Sofja Kovalevskaya Award of Alexander von Humboldt Foundation.

Keywords: doping · electron microscopy · ferroelectrics · oxygen vacancies · perovskite defects

How to cite: *Angew. Chem. Int. Ed.* **2015**, *54*, 14787–14790
Angew. Chem. **2015**, *127*, 15000–15003

[1] B. Jaffe, W. R. Cook, H. Jaffe, *Piezoelectric Ceramics*, Academic Press, London, **1971**.
[2] T. R. N. Kutty, R. Balachandran, *Mater. Chem. Phys.* **1985**, *13*, 467–475.
[3] D. J. Keeble, M. Loyo-Menoyo, Z. I. Y. Booq, R. R. Garipov, V. V. Eremkin, V. Smotrakov, *Phys. Rev. B* **2009**, *80*, 1–7.
[4] R. A. Eichel, *J. Electroceram.* **2007**, *19*, 9–21.
[5] H. Meštrić, R. A. Eichel, K. P. Dinse, A. Ozarowski, J. Van Tol, L. C. Brunel, *J. Appl. Phys.* **2004**, *96*, 7440–7444.
[6] A. Chandrasekaran, D. Damjanovic, N. Setter, N. Marzari, *Phys. Rev. B* **2013**, *88*, 1–7.
[7] J. F. Scott, M. Dawber, *Appl. Phys. Lett.* **2000**, *76*, 3801–3803.
[8] M. Dawber, J. F. Scott, *Appl. Phys. Lett.* **2000**, *76*, 1060–1062.
[9] X. J. Lou, *J. Appl. Phys.* **2009**, *105*, 024101.
[10] M. Dawber, K. M. Rabe, J. F. Scott, *Rev. Mod. Phys.* **2005**, *77*, 1083–1130.
[11] A. K. Tagantsev, I. Stolichnov, E. L. Colla, N. Setter, *J. Appl. Phys.* **2001**, *90*, 1387–1402.
[12] A. H. Meitzler, *Ferroelectrics* **1976**, *11*, 503–510.
[13] A. M. Abakumov, J. Hadermann, S. Bals, I. V. Nikolaev, E. V. Antipov, G. Van Tendeloo, *Angew. Chem. Int. Ed.* **2006**, *45*, 6697–6700; *Angew. Chem.* **2006**, *118*, 6849–6852.
[14] A. M. Abakumov, J. Hadermann, G. Van Tendeloo, E. V. Antipov, *J. Am. Ceram. Soc.* **2008**, *91*, 1807–1813.
[15] J. Hadermann, A. M. Abakumov, I. V. Nikolaev, E. V. Antipov, G. Van Tendeloo, *Solid State Sci.* **2008**, *10*, 382–389.
[16] A. M. Abakumov, D. Batuk, J. Hadermann, M. G. Rozova, D. V. Sheptyakov, A. A. Tsirlin, D. Niermann, F. Waschkowski, J. Hemberger, G. Van Tendeloo, *Chem. Mater.* **2011**, *23*, 255–265.
[17] D. Batuk, M. Batuk, A. M. Abakumov, A. A. Tsirlin, C. McCammon, L. Dubrovinsky, J. Hadermann, *Inorg. Chem.* **2013**, *52*, 10009–10020.
[18] D. Batuk, M. Batuk, A. M. Abakumov, J. Hadermann, *Acta Crystallogr. Sect. B* **2015**, *71*, 127–143.
[19] H. Mestrić, R. A. Eichel, T. Kloss, K. P. Dinse, S. Laubach, S. Laubach, P. C. Schmidt, K. A. Schönau, M. Knapp, H. Ehrenberg, *Phys. Rev. B* **2005**, *71*, 1–10.
[20] P. Erhart, R. A. Eichel, P. Träskelin, K. Albe, *Phys. Rev. B* **2007**, *76*, 1–12.
[21] H. Ganegoda, J. A. Kaduk, C. U. Segre, *Powder Diffr.* **2013**, *28*, 238–245.
[22] V. Petříček, M. Dusek, L. Palatinus, *Z. Kristallogr.* **2014**, *229*, 345–352.

Received: August 18, 2015
Published online: October 21, 2015

